buildings

MDPI

Article

Reliability Analysis of Axial Compressive Strength of Concrete-Filled Steel Tube (CFST) under Coupled Corrosion and Load Effects

Dan-Yang Ma [1,2], Shuai Ma [1] and Li-Yan Xu [1,2,*]

[1] School of Transportation Science and Engineering, Beihang University, Beijing 100191, China; madanyang@buaa.edu.cn (D.-Y.M.); ma17837026960@buaa.edu.cn (S.M.)
[2] Key Laboratory of Intelligent Transportation Technology and System, Ministry of Education, Beijing 100191, China
* Correspondence: xuliyan@buaa.edu.cn

Abstract: This paper presents a finite element analysis (FEA) of and reliability study on concrete-filled steel tube (CFST) members under the combined effects of corrosion and compressive loading. First, a stochastic-based FE model is established through the proposed secondary development program based on ABAQUS 2021 software. The model could account for the uncertainties of material, geometric, and corrosion effect on CFST members. The reliability of the built model was validated through experimental data of corroded CFST members under compression loading. Subsequently, the compressive performance of CFST under a combination of corrosion and loading was further investigated by numerical parameter analysis. A total of 1800 models were created to clarify the coupling mechanism among the core concrete strength, the steel tube strength, the steel ratio, and the maximum strength of the CFST member. Three theoretical formulas presented in classical design standards were used to calculate the axial compressive strength of the corroded CFST, and the uncertainty parameters μ_{kp} and δ_{kp} were also obtained for the discussed design formulas. Finally, the First Order and Second Moment (FOSM) method was employed to estimate the reliability indices β across different standards. The calculations revealed that the reliability indices β according to European standard ranges from 2.93 to 5.52, with some results falling below the target reliability index β_T of 3.65. In addition, the multi-parameter coupling effects on reliability index β were investigated, and the main influencing factors were obtained. By leveraging the reliability analysis, reasonable design requirements can be proposed for CFST members under the coupling effects of corrosion and external load, which provides a design basis for the CFST member.

Keywords: concrete-filled steel tube; parametric modelling; stochastic-based modelling; axial compressive strength; reliability index

Citation: Ma, D.-Y.; Ma, S.; Xu, L.-Y. Reliability Analysis of Axial Compressive Strength of Concrete-Filled Steel Tube (CFST) under Coupled Corrosion and Load Effects. *Buildings* **2024**, *14*, 3205. https://doi.org/10.3390/buildings14103205

Academic Editor: Duc-Kien Thai

Received: 8 September 2024
Revised: 3 October 2024
Accepted: 7 October 2024
Published: 9 October 2024

1. Introduction

Concrete-filled steel tube (CFST) structures are widely used in engineering, particularly in high-rise buildings and large-span bridges [1]. The confinement effects from the steel tube enable CFST structures to exhibit favourable strength, stiffness, and ductility when subjected to extreme loads. However, the mechanical performance of CFST structures may be affected by stochastic factors in practical engineering, such as external loads, material strength, and steel tube corrosion. This uncertainty highly affects structural safety and reliability and poses challenges for engineering practise. Taking CFST members as an example, steel tubes may experience varying degrees of corrosion in a wet environment, as illustrated in Figure 1. The main impact of corrosion results in a reduction in steel tube thickness, leading to a decrease in the strength, durability, and reliability of the CFST structure [2]. Therefore, it is necessary to consider not only the structural strength under external loads but also the coupling effects of corrosion and external load.

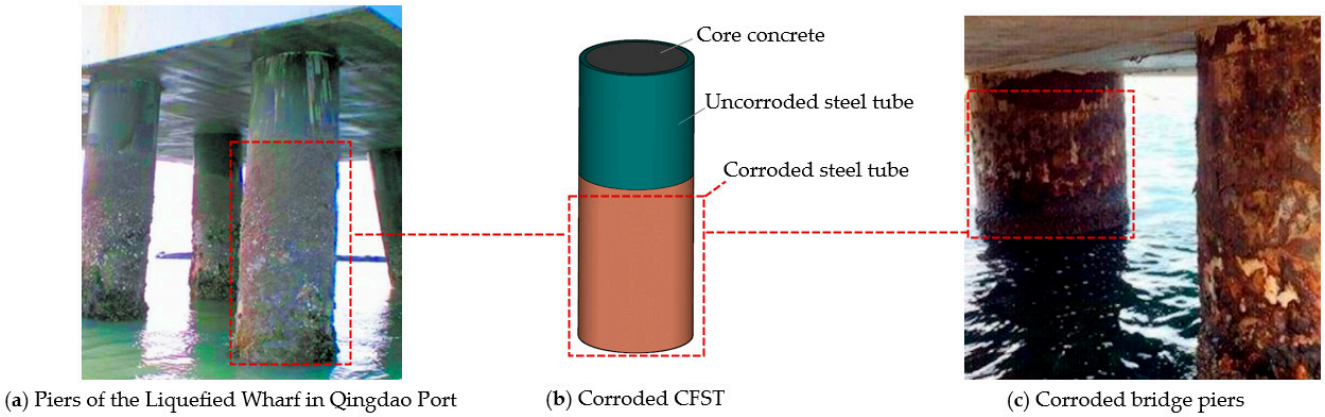

Figure 1. Corrosion of CFST structures in actual engineering structures [3].

Many studies have been conducted on the corrosion of steel materials, as reported in the literature. Almusallam [4] investigated the impact of corrosion on the performance of steel reinforcement, finding that tensile strength decreased slightly with increasing corrosion levels and the steel reinforcement exhibited brittle failure when the corrosion rate exceeded 12.6%. Qin and Cui [5] proposed a novel corrosion model that accounts for the corrosion process of steel structures and examined its impact on time-dependent reliability. Their study highlighted the superiority and flexibility of the proposed model. However, when CFST structures are corroded, they often exhibit obvious corrosion on the outer surface while experiencing inapparent corrosion on the inner surface. Different from the steel plates, the curvature of the steel tube would lead to greater unevenness and randomness under corrosion. The corrosion behaviour in CFST differs significantly from that of steel reinforcement and plates, and there is a lack of reliability analysis results for circular CFST corrosion.

Previous studies on CFST corrosion often analyzed the effects of corrosion and loading separately. Li [6] conducted axial compression tests on 21 CFST specimens with varying degrees of corrosion and observed the failure mode of the steel tube local buckling. The axial compressive strength and stiffness of CFSTs were influenced by both the corrosion ratio, corrosion area, and corrosion ratio. Based on these findings, a method for predicting the axial compressive strength of corroded CFST was proposed, which showed good agreement with experimental results. Yang [7] investigated the axial compressive strength of CFST under corrosion, developing a finite element model for corroded CFST, and introduced a strength reduction factor to calculate the axial compressive strength after corrosion. By studying the influence of variables such as material strength, steel tube thickness, and dimensions, a formula for calculating the axial load-bearing capacity under corrosion conditions was proposed. Zhang et al. [8] investigated the influence of steel tube corrosion on the strength of circular thin-walled CFST members. Different levels of corrosion were induced on the steel tubes through accelerated corrosion methods. Experimental results indicated that the strength of the CFST structures decreased with the increase in corrosion. The failure mode was characterized by typical shear expansion accompanied by slight local buckling. Li et al. [9] established an FE model of a double-layer CFST and investigated its mechanical properties after continuous loading and chloride corrosion, finding a significant strength decrease in CFST post corrosion. For the reliability analysis of CFST structures, the First Order and Second Moment (FOSM) method is widely applied by researchers. Considering the effects of initial defects and steel tube corrosion, Han et al. [10] proposed an FE model for CFSTs based on the entire life cycle and employed the FOSM method to calculate the reliability. They also presented a reliability calculation method that meets current design standards. However, CFST often endure corrosion and loading simultaneously in practical engineering. The coupling of these two effects remains unclear, causing potential safety hazards.

In spite of extensive studies on the mechanical performance and reliability analysis of CFST members in the literature, the topic of the compressive behaviour of CFST members under coupled effect of corrosion and load has not been fully addressed. The main problems include the following:

(1) The distribution types and patterns of corrosion in CFST members are not yet clear, and there is limited research on the uncertainty parameters of circular steel tube corrosion.
(2) Previous research has primarily focused on the impact of isolated steel tube corrosion, lacking comprehensive studies on the coupling effects of steel tube corrosion and external loads.
(3) In terms of reliability analysis methods, current research tends to use empirical uncertainty parameters and the FOSM method to calculate reliability indices. However, there is still a lack of reasonable reliability analysis methods based on refined FE analysis.

To address the gaps in previous research, this paper establishes a refined FE model of CFST members based on random distribution, which can account for the uncertainties of steel tube corrosion and other variables. Based on this, the mechanical performance of CFST members under the combined effects of loading and corrosion is analyzed, and construction requirements could finally be proposed.

2. Establishment of the FE Model

To analyze the strength and reliability of CFST members under corrosion and external loads, this study developed a stochastic-based FE model. The random distribution of the material strength, dimension, and external load is incorporated into the model by secondary development with Python.

This study primarily investigated the axial compressive strength and reliability of CFST members under corrosion and axial compressive loads. To establish the boundary conditions, the bottom of the CFST member was constrained by setting U1 = U2 = U3 = 0 and UR1 = UR2 = UR3 = 0. Axial loading was applied at the top of the CFST members to simulate the external load, as illustrated in Figure 2a. In order to express the coupling process of force and corrosion, the loading and corrosion processes occur in three steps as follows: ① An external load N_1 is applied to the CFST member, representing the construction and service load, generating internal forces and deformations. ② While sustaining the external load, corrosion continues to work on the outer surface of the steel tube, primarily reducing its thickness. ③ With the external load increasing, an ultimate load N_u is applied to the CFST member, leading it to the ultimate state. The load ratio η is defined as the ratio between the normal external load N_1 and the maximum strength N_u of the CFST member. The load–displacement relationship of the whole process is depicted in Figure 2b. Considering the effects of corrosion and load, the maximum strength of the CFST member may decrease, and additional deformation may occur during the loading process.

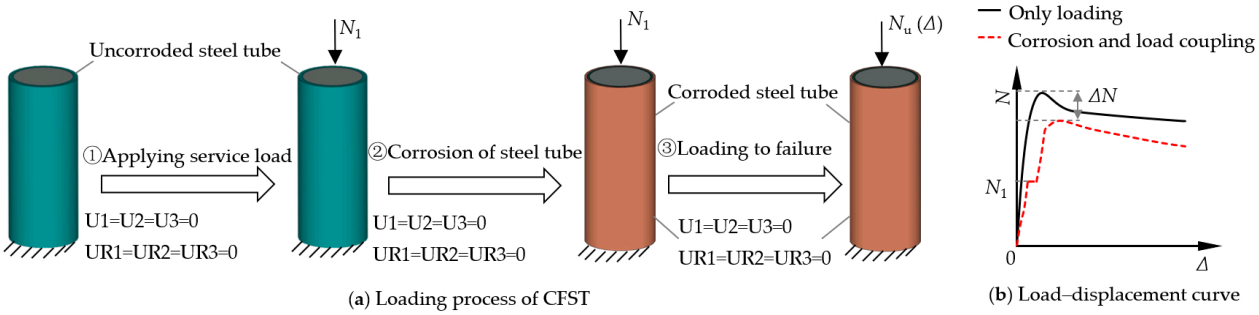

Figure 2. Schematic of loading and corrosion of CFST.

In FE modelling, the cross-section could be divided into three regions: the corroded outer steel tube (yellow), the uncorroded inner steel tube (green), and the internal core

concrete (grey). The corrosion procedure is shown in Figure 3b. The region of the corroded area of the outer steel tube would gradually decrease with the development of corrosion, corresponding to stage ② in Figure 2.

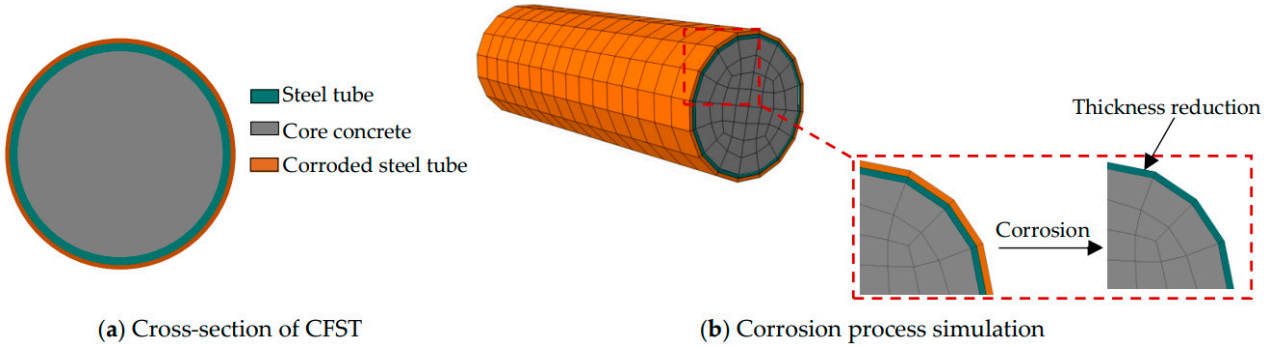

(**a**) Cross-section of CFST (**b**) Corrosion process simulation

Figure 3. Schematic of CFST corrosion simulation.

2.1. Constitutive Model, Mesh, and Interaction

(1) Constitutive model

The constitutive model is crucial for ensuring calculation accuracy and computational efficiency. In this study, the concrete damaged plasticity model (CDP model) was employed for concrete, assuming that the primary mechanisms of concrete failure were tensile cracking and compressive crushing. This model is applicable for analyzing concrete at low confining pressures.

This study exclusively examined the mechanical properties under axial compressive loading. Therefore, the CDP model had the following basic mechanical parameters: the E_c of concrete was taken as $4730\sqrt{f_c'}$, and Poisson's ratio was assumed to be 0.2. Due to the confinement effect of the steel tube, the stress–strain relationship for the core concrete under axial compression was modelled as recommended by Han [11]. The following formula is applicable:

$$y = \begin{cases} 2x - x^2 & (x \le 1) \\ \frac{x}{\beta \cdot (x-1)^2 + x} & (x > 1) \end{cases} \quad (1)$$

The confinement effect of the steel tube has a negligible influence on the tensile performance of the core concrete. Thus, the tensile stress–strain relationship model proposed in GB50010-2010 [12] can be directly utilized for the core concrete.

A steel tube is typically made of low-carbon steel or low-alloy structural steel, characterized by a distinct yield plateau and hardening stages. The elastic modulus Es of steel was taken as 206,000 N/mm^2, and Poisson's ratio was assumed to be 0.3. In this study, the five-stage stress-strain relationship proposed by Han [11] was utilized to characterize the axial stress-strain behaviour of the steel tube. This model effectively accounts for the plastic flow and strength hardening of the steel material.

(2) Mesh

In FE analysis, appropriate element types and meshes are crucial. Concrete is represented using standard hexahedral solid elements (C3D8R). Although previous studies mainly used shell elements to simulate the steel tube, this model employs solid elements for the steel tube to account for its complex geometry when corroded. To ensure the proper contact relationship and improve computational convergence, it is necessary to ensure that the mesh nodes of the components in contact correspond to each other at the contact locations. Specifically, the outermost elements of the core concrete must spatially overlap completely with the innermost elements of the steel tube, as shown in Figure 3b. Finally, the mesh density is critical in computational modelling, as it significantly impacts both accuracy and computational efficiency. Before determining the mesh density, various denser and sparser meshes were tested. Finally, the outer diameter of the steel tube was

determined to be 1000 mm, and the length was 3000 mm, with 16 meshes arranged around the circumference of the steel tube. To maintain a balanced mesh size, the mesh density was uniformly applied across all dimensions.

(3) Interaction

The interaction has a significant impact on the accuracy and convergence of FE analysis. In CFST members, the only interaction is the interface between the steel tube and the core concrete. The normal interaction adopts "Hard Contact", and the frictional resistance between the two materials is described by a "Friction" model. The friction coefficient μ is set as a constant value of 0.6.

2.2. Verification of FE Model

To verify the accuracy of the FE model calculations, the experimental results of the corroded steel tube were compared with the simulated results, including the failure modes and force–displacement relationship, which can be found in Figures 4 and 5. Chen [13] conducted axial compressive tests on five short CFSTs after acid rain corrosion, as shown in Figure 4a. Specimen C-114-2 had a corrosion rate of 0.205 and exhibited buckling of the outer steel tube at the ultimate state. To investigate the effects of severe cold and acid rain on the mechanical properties of square CFSTs, Zhang [14] conducted axial compression experiments on specimen S4.5-0-10 under a temperature of 0 °C and a corrosion rate of 0.10. During the loading process, the core concrete was subjected to a continuously increasing axial load until it crushed, as shown in Figure 4b. The observed failure modes of steel tube and concrete are consistent with the FE analysis results, indicating that the FE model can accurately simulate the failure mode of CFST members under load and corrosion.

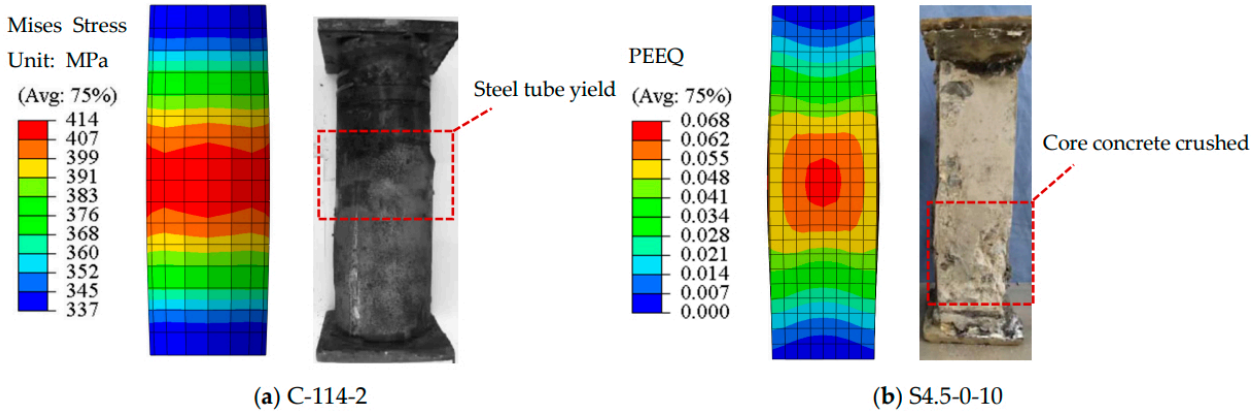

Figure 4. Verification of failure modes [13,14].

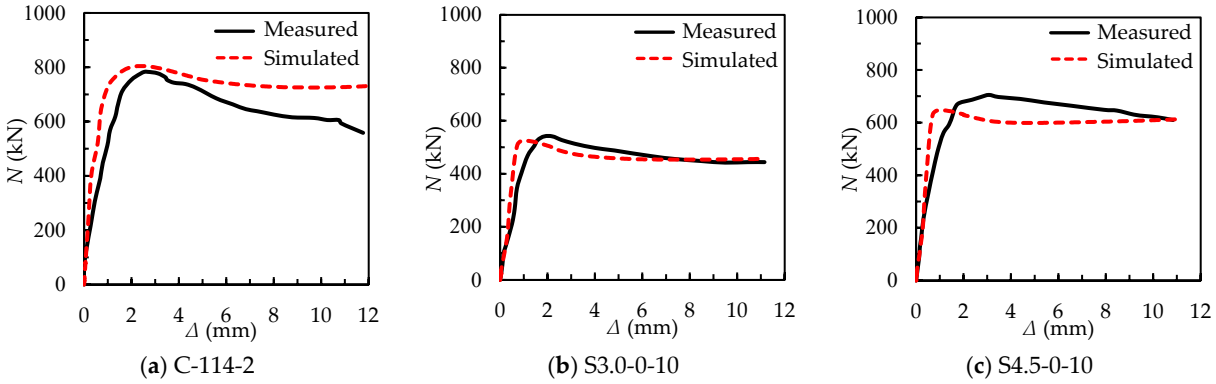

Figure 5. Verification of axial force (N)–axial displacement (Δ) relationship [13,14].

The axial force (N)–axial displacement (Δ) relationship from the FE models and experimental measurements are shown in Figure 6. The solid black lines represent the measured

relationship, while the dashed red lines depict the FE-simulated relationship. The results show that the simulated axial compressive strength is close to the measured strength, and there is a high degree of consistency between the two force–displacement curves. However, the initial stiffness obtained from the FE simulation is slightly higher than the measured one, which could be attributed to the presence of minor displacements and contact gaps during experimental loading. Despite this discrepancy, it does not significantly impact the prediction strength.

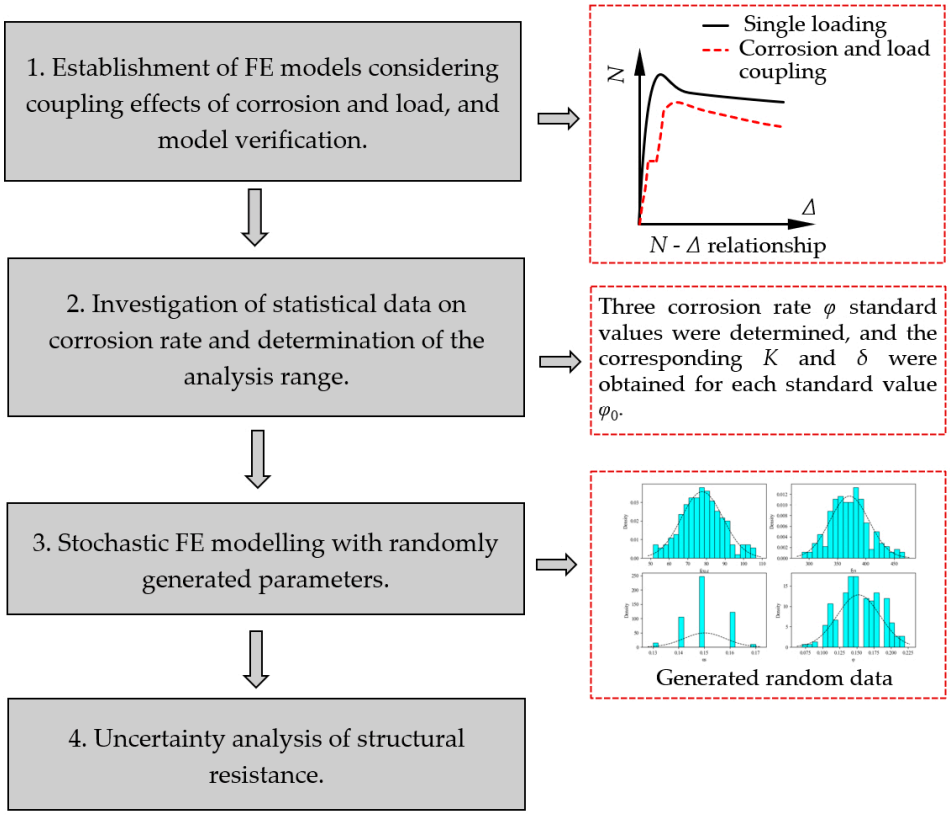

Figure 6. Procedure for stochastic FE modelling.

2.3. Uncertainty of FE Model

2.3.1. Uncertain Variables of Material and Geometry

It is essential to identify the uncertainties inherent in the FE model when conducting the reliability analysis of CFST members. For CFST members, these uncertainties primarily encompass material properties, geometric parameters, load conditions, and the corrosion rate. According to previous statistical results on material strength, the yield strength of steel tube and the cube strength of core concrete followed the normal distribution [12]. The uncertain variables were investigated by previous researchers and can be referenced from the latest monograph [11], as shown in Tables 1 and 2, respectively.

Table 1. Uncertain variables of concrete.

K	***δ***	***K***	***δ***	***K***	***δ***	***K***	***δ***
C30		C40		C50		C60	
1.395	0.172	1.345	0.156	1.325	0.149	1.302	0.141

Note: K is the ratio of the mean to the standard value, and δ is the coefficient of variation. When the concrete strength grade is greater than C60, take K = 1.302 and δ = 0.141.

Table 2. Uncertain variables of steel.

K	*δ*	*K*	*δ*	*K*	*δ*	*K*	*δ*
Q235		Q355		Q420		Q460	
1.28	0.095	1.05	0.082	0.96	0.099	0.96	0.087

Note: K is the ratio of the mean to the standard value, and δ is the coefficient of variation.

The uncertainty of geometric parameters is generally determined through statistical results from various structural components. In this study, the steel tube ratio α_s is defined in Equation (2) and is summarized as a normal distribution with a mean value K of 1.00 and a standard deviation δ of 0.05:

$$\alpha_s = A_s / A_c \tag{2}$$

where A_c represents the cross-section area of the core concrete in the CFST, and A_s represents the cross-section area of the steel tube in the CFST.

2.3.2. Uncertain Variables of Load

This study examined three primary structure design standards: the American AASHTO [15], European Eurocode 0:2005 [16], and Chinese GB 50068-2018 [17]. The dead load probability model typically follows a normal distribution in AASHTO, with a K of 1.03 and δ of 0.08. Similarly, the probability model of live loads also exhibits a normal distribution, with K at 1.29 and δ at 0.18. The American code also outlines the relationship between resistance and load combinations at the ultimate limit state for strength as follows:

$$R_n / \gamma_n = \gamma_D D_n + \gamma_L L_n \tag{3}$$

In this equation, R_n represents structural resistance, and D_n and L_n are the dead load and live load, respectively. γ_n is the resistance partial factor, while γ_D and γ_L are the partial factors for the dead load and live load, respectively, with values of 1.25 and 1.75.

In Eurocode 0:2005, the combination of dead load and live load effects is considered in a similar way, and the expression is as follows:

$$R_k / \gamma_R = \gamma_D D_k + \gamma_L L_k \tag{4}$$

In this equation, R_k represents the structural resistance, and D_k and L_k represent the dead load and live load, respectively. γ_R stands for the resistance partial factor, where γ_D = 1.35 and γ_L = 1.35. The probability models for dead and live loads can be adopted from AASHTO [18].

In GB 50068-2018, the combination of effects is similarly utilized to obtain the combination expression as follows:

$$R_k / \gamma_R = \gamma(\gamma_D D_k + \gamma_L L_k) \tag{5}$$

In this equation, γ_D = 1.20 and γ_L = 1.40, where γ represents the structural importance factor, which is assumed to be 1.0 for secondary-level structures.

In highway bridge and culvert engineering, dead loads are typically modelled using a normal distribution. While live loads generally follow either a normal distribution or an extreme value distribution model of type I. This distribution model is primarily employed to analyze the occurrence probabilities of extreme events, such as extreme weather conditions and live loads, and is of significant practical importance.

In this study, the most adverse live load type was selected for analysis. According to the statistical parameters outlined in Chinese standard GB/T 50283-1999 [19], the vehicle load was chosen as the live load distribution type. Additionally, vehicle loads may experience extreme scenarios that significantly affect structural reliability. Therefore, it is emphasized that an extreme value distribution model of type I is chosen for live loads.

Summarizing the above three different national standards, we could obtain the parameters of load uncertainty from different standards. Table 3 presents the statistical results. It is generally recognized that there is a certain load ratio η between the live load and dead load. According to the building structural engineering, three different load ratios η were set in this study: 0.20, 0.40, and 0.60.

Table 3. Uncertain variables of load.

Standard	Partial Factor for Dead Load γ_D	Partial Factor for Live Load γ_L	Dead Load Uncertainty		Live Load Uncertainty	
			K	δ	K	δ
AASHTO	1.25	1.75	1.03	0.08	1.29	0.18
Eurocode 0:2005	1.35	1.35	1.03	0.08	1.29	0.18
GB 50068-2018	1.20	1.40	1.015	0.431	0.800	0.086

2.3.3. Uncertain Variables of Corrosion

Considering the uncertainties in all aspects, existing research lacks thorough statistics on the uncertainty of the corrosion rate and the corresponding statistical parameters. Therefore, a detailed investigation of previous studies was conducted in this study to quantify these uncertainties. To investigate the mechanical properties of CFST members after acid rain corrosion, Chen [13] immersed all experimental specimens in a solution to simulate the effects of acid rain corrosion, assuming that the variation in the thickness of the outer steel tube was uniform. In this study, the corrosion model employed by Chen [13] was adopted, and the corrosion rate is defined as φ:

$$\varphi = \frac{\Delta t}{t_0} \tag{6}$$

where Δt represents the corroded thickness of the steel tube, and t_0 represents the original thickness of the steel tube.

The cross-sectional area of the corroded steel tube, denoted as A_s, can be expressed as follows:

$$As = \frac{\pi}{4}\left[(D - 2\Delta t)^2 - (D - 2t_0)^2\right] \tag{7}$$

where D denotes the outer diameter of the steel tube.

In using Equations (6) and (7), the cross-sectional area of the steel tube after corrosion can be determined. Subsequently, the effects of corrosion are incorporated into the calculation of axial compressive strength.

Table 4 displays the statistical data collected from previous studies regarding the corrosion rate. By thoroughly analyzing these data, the distribution patterns and variability of φ can be determined, leading to a more precise reliability analysis of the corrosion rate. The tests of uniform corrosion were investigated in previous studies. Compared with the non-uniform corrosion, the uniform corrosion could also reflect the reduction in the thickness of corroded steel tubes and weakened confinement effect, which is the key factors affecting mechanical properties. Therefore, uniform corrosion was applied in the numerical study.

It was found that many scholars use an electric current method to accelerate the corrosion of steel tubes, aiming to save experimental time [20,21]. The corrosion rate is influenced by the duration and intensity of the current. Therefore, three sets of corrosion rate standard values (φ_0 = 0.15, 0.25, and 0.40) were obtained from uniformly corroded data, as shown in Table 4, considering different current durations and intensities. Based on the statistical results, the uncertain parameters under different corrosion rates were calculated. The calculation results are shown in Table 5.

Table 4. Statistics on the corrosion degree.

Reference	Specimen Name	Diameter of Steel Tube D (mm)	Thickness of Steel Tube t_s (mm)	Corrosion Rate φ
Chen et al. [13]	C-114-1	113.50	2.65	0.095
	C-114-2	112.92	2.65	0.205
	C-140-2	138.98	2.59	0.196
Hua [20]	St1	140	3.67	0.302
	St2	140	3.67	0.256
	St4	140	3.67	0.185
	St5	140	3.67	0.226
	St7	140	3.67	0.158
	Sbc1	140	3.67	0.150
	Sbc2	140	3.67	0.155
	Sbc4	140	3.67	0.084
	Sbc5	140	3.67	0.183
	Sbc7	140	3.67	0.087
	Sbch1	140	3.67	0.161
	Sbch3	140	3.67	0.204
	Sbch4	140	3.67	0.150
Han et al. [21]	ct1-1	160	3.92	0.406
	ct1-2	160	3.92	0.273
	ct2-1	160	3.92	0.457
	ct2-2	160	3.92	0.291
	ct4-1	160	3.92	0.186
	ct4-2	160	3.92	0.181
	cht1-1	160	3.92	0.459
	cht1-2	160	3.92	0.375
Li et al. [6]	A10-22	76	3.00	0.10
	A10-44	76	3.00	0.10
	A20-22	76	3.00	0.20
	A20-44	76	3.00	0.20
	A30-22	76	3.00	0.30
	A30-44	76	3.00	0.30

Table 5. Uncertain parameters for different corrosion rate standard values.

Corrosion Rate Standard Values φ_0	Mean Value μ	Standard Deviation σ	Ratio of Mean to Standard Value K	Coefficient of Variation δ
0.15	0.153	0.034	1.020	0.222
0.25	0.259	0.035	1.036	0.135
0.40	0.424	0.035	1.060	0.083

In summary, the uncertainty parameters of the corrosion rate were determined through the investigation of previous statistical data. Establishing the uncertain parameters related to the corrosion rate not only provides crucial data for the stochastic FE models but also lays the essential groundwork for subsequent reliability analysis.

2.4. Modelling Procedure Based on Stochastic Distribution

Table 6 outlines the specific parameter values for the FE model, including load ratios of 0.20, 0.40, and 0.60, and corrosion rates of 0.15, 0.25, and 0.40. The stochastic FE modelling procedure is summarized in Figure 6. Firstly, establish an FE model capable of simulating the full range of the corrosion and loading. Moreover, verify the FE model using the test results. Secondly, investigate statistical data on corrosion rates to obtain the mean-to-standard value ratio K and coefficient of variation δ for each corrosion rate φ_0. Random distributions of other parameters, including the load ratios, cube strength of the core concrete, yield strength of the steel tube, and steel tube ratio, are also considered. Thirdly,

perform stochastic FE modelling using Python programming. In total, 200 sets of random data were generated for each standard corrosion rate value. With consideration for three load ratios, a total of 1800 FE models incorporating corrosion were established. As the fourth and final point, analyze the reliability of the corroded CFST members, considering the randomness of the five aforementioned parameters, with a focus on the effects of corrosion and loading. Furthermore, it could provide essential statistical results for further reliability analysis.

Table 6. The FE model's parameter ranges.

Uncertain Parameters	Parameter Range
Load ratio η	0.20, 0.40, 0.60
Cube strength of the core concrete $f_{cu,c}$ (MPa)	60
Yield strength of the steel tube f_{ys} (MPa)	355
Steel tube ratio α_s	0.15
Corrosion rate standard values φ_0	0.15, 0.25, 0.40

3. Structural Resistance Uncertainty Considering Corrosion Effect

With the established stochastic-based FE model, the uncertainty analysis of corroded CFST members could be conducted. It is essential to identify the critical parameters that most significantly affect compressive strength, providing a basis for further reliability analysis.

3.1. Influence of Corrosion on Structural Resistance

Taking load ratio η of 0.20 as an example, the coupling effects of $f_{cu,c}$, f_{ys}, α_s, and φ_0 were analyzed with the established stochastic FE model. Due to the limitations on the display dimensions, only three critical parameters under different φ_0 values could be displayed in 3D graphics, as depicted in Figure 7. The 3D graphics could visually display coupling effects on the maximum strength N_u. Additionally, projections onto XZ (gray) and YZ (green) planes were created to enhance the visualization of the influence patterns of particular parameters. Subsequently, identifying the parameter with the most significant influence on N_u is helpful. Finally, an investigation was conducted to figure out the interaction between this key parameter and the corrosion rate φ on the maximum strength N_u.

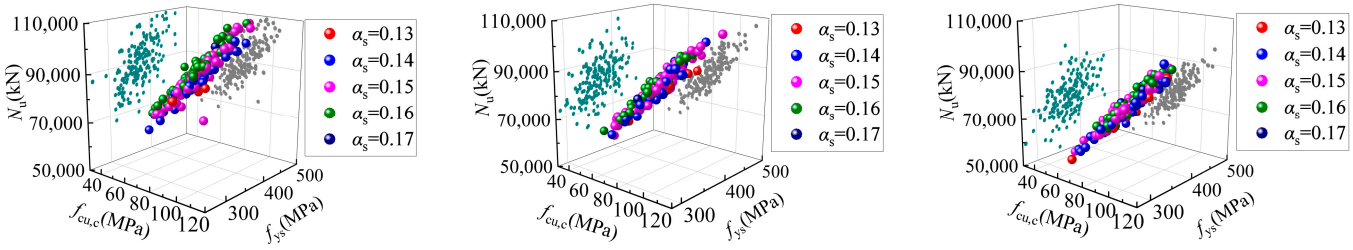

(**a**) φ_0 = 0.15 (**b**) φ_0 = 0.25 (**c**) φ_0 = 0.40

Figure 7. The influence of various parameters on N_u.

Figure 7 depicts the coupling influence patterns of various parameters on N_u under the corrosion rates of 0.15, 0.25, and 0.40, respectively. The randomly generated steel tube ratio α_s ranges from 0.13 to 0.17. It is evident that N_u is mainly affected by $f_{cu,c}$ and f_{ys}, with the influence of the minimal value of α_s. This is due to the slight variation in α_s in the CFST after corrosion, leading to the other two parameters being remarkable. The consistency in the influence patterns of $f_{cu,c}$ and f_{ys} can be observed under different corrosion rates. Taking φ_0 = 0.15 as an example, a representative analysis was conducted, as depicted in Figure 7a. The maximum strength N_u increases by 53.30% at most with the increase in $f_{cu,c}$.

Although an increase in f_{ys} also leads to an increase in N_u, the impact is less significant compared to that in $f_{cu,c}$. Another reason is that the steel tube occupies a relatively small proportion of the CFST cross-section. The majority of the cross-sectional area consists of the core concrete, which bears most of the load. Consequently, maximum strength N_u is primarily influenced by $f_{cu,c}$.

Since the $f_{cu,c}$ has the most significant impact on the maximum strength N_u, it was selected to analyze the coupling effects with corrosion rate φ on N_u, as illustrated in Figure 8. As mentioned above, the influence of φ changes with the variation in $f_{cu,c}$. To further investigate this coupling effect, the analytical results were divided into two groups according to $f_{cu,c}$ for detailed analysis. When the corrosion rate standard value is 0.15, N_u increases with increasing $f_{cu,c}$. Specifically, when $f_{cu,c}$ increases from 40 MPa to 80 MPa, N_u increases by 36.21% and decreases by 7.60% as φ increases. Similarly, when $f_{cu,c}$ increases from 80 MPa to 110 MPa, N_u increases by 21.61%, with a slight 1.03% decrease as φ increases. For a corrosion rate standard value of 0.25, N_u increases by 27.25% and 15.24% as $f_{cu,c}$ varies within 40 MPa to 80 MPa and 80 MPa to 110 MPa, respectively. Conversely, N_u decreases by 17.75% and 12.71% as φ increases. The observed trend persists for a corrosion rate standard value of 0.40, where the N_u exhibits an increase with $f_{cu,c}$ and a decrease with φ. That trend becomes more significant when the compressive strength $f_{cu,c}$ is below 80 MPa.

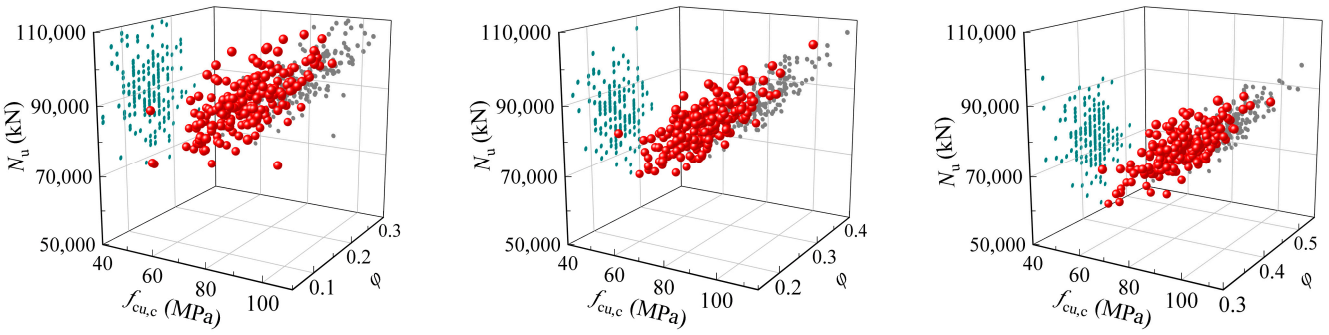

(**a**) $\varphi_0 = 0.15$ (**b**) $\varphi_0 = 0.25$ (**c**) $\varphi_0 = 0.40$

Figure 8. The influence of φ and $f_{cu,c}$ on N_u.

In summary, the maximum strength N_u is greatly affected by $f_{cu,c}$ and φ. Moreover, the influence of various material and geometric parameters becomes more prominent with a higher corrosion rate φ. Severe corrosion can significantly reduce the thickness of the steel tube, which not only further decreases the strength of the steel tube but also weakens the confinement of the core concrete. When the confinement decreases, the compressive strength of the core concrete is adversely affected, leading to a reduction in compressive strength of the CFST member. For instance, the analysis indicates that, as corrosion progresses when the standard corrosion rate of the steel tube is set at 0.25. The axial compressive strength of the CFST members decreases with an additional 10.15% and 11.68% compared to the standard corrosion rate of 0.15. This indicates that corrosion rate φ not only has a direct impact on axial compressive strength but also interacts significantly with other factors, highlighting the need for a reliability assessment of axial compressive strength under varying corrosion rates.

3.2. Uncertainty Variables of Structural Resistance

In the calculation of the axial compressive strength of CFST, Chinese standard DBJ/T13-51-2010 [22], American standard AISC 360-16 [23], and European standard Eurocode 4:2004 [24] are all from comparable time periods, enabling a comparative analysis on strength calculation formulas. Since the calculation formulas from DBJ/T13-51-2010 [22] have been incorporated into the international version of GB/T 51446-2021 [25], this study

employed Chinese standard GB/T 51446-2021 to calculate and compare the axial compressive strength of CFST. The relevant formulas are presented in Table 7.

Table 7. Calculation methods for axial compressive strength.

Standard	Formula	
GB/T 51446-2021 [25]	$N_{cfst} = \frac{(1.14+1.02\xi)f_{ck}A_{sc}}{\gamma}$	(8)
AISC 360-16 [23]	$N_{cfst} = f_{ys}\ A_s + 0.85f_c'A_c$	(9)
Eurocode 4:2004 [24]	$N_{cfst} = \eta_a\ f_{ys}\ A_s + f_c'A_c\left(1 + \eta_c \cdot \frac{t}{D} \cdot \frac{f_{ys}}{f_{ck}}\right)$	(10)

Note: N_{cfst}—compressive strength of CFST (N); f_{ck}—characteristic strength of concrete (MPa); f_c'—cylinder compressive strength of concrete (MPa); f_{ys}—yield strength of steel tube (MPa); A_c—cross-sectional area of core concrete in CFST (mm^2); A_s—cross-sectional area of steel tube in CFST (mm^2); A_{sc}—cross-sectional area of CFST (mm^2); ξ—confinement factor ($\xi = \frac{A_s f_y}{A_c f_{ck}}$).

The axial compressive strength of 1800 aforementioned CFST models was calculated according to those three different standards. The FE model was verified by the test results and could directly account for the coupling effect of corrosion and load. Therefore, it was regarded as an accurate result. To compare the standards objectively, the reduction in steel tube thickness caused by the corrosion was considered in the standard calculations. This reduction affected the variables of A_s, A_{sc}, and ξ in the standard calculations. However, the standard could not account for the coupling of corrosion and external load. The FE-simulated value of N_s represented measured strength, and the standard-calculated value of N_0 represented the calculated strength. The uncertainty parameter k_p of the calculation methods is shown in Equation (11):

$$k_p = \frac{N_s}{N_0} \tag{11}$$

Based on the results of numerous FE model calculations and the standard calculations, the mean μ_{kp} and coefficient of variation δ_{kp} under different external loads and corrosion rates were obtained, as shown in Table 8. The calculation uncertainty parameter k_p was summarized for different load ratio η and corrosion rate φ. It could be found that the mean μ_{kp} usually increased a bit as the load ratios η decreases and the corrosion rate φ increases. This indicates that the standard could not fully account for the coupling effects of force and corrosion on the reduction in structural strength. With comparisons among the three standards, AISC 360-16 [23] underestimates the axial strength after corrosion, and Eurocode4: 2004 [24] overestimates the axial strength after corrosion in general. Nevertheless, GB/T 51446-2021 [25] presents the appropriate results and determines the minimum coefficient of variation.

Table 8. Uncertainty parameters of calculation methods.

Load Ratio η	Corrosion Rate Standard Value φ_0	GB/T 51446-2021		AISC 360-16		Eurocode4: 2004	
		μ_{kp}	δ_{kp}	μ_{kp}	δ_{kp}	μ_{kp}	δ_{kp}
0.20	0.15	1.060	0.018	1.269	0.023	0.945	0.026
	0.25	1.065	0.018	1.258	0.024	0.945	0.025
	0.40	1.067	0.015	1.237	0.024	0.948	0.026
0.40	0.15	1.059	0.018	1.269	0.023	0.945	0.025
	0.25	1.068	0.017	1.264	0.024	0.951	0.027
	0.40	1.072	0.017	1.244	0.025	0.954	0.026
0.60	0.15	1.058	0.016	1.268	0.020	0.944	0.024
	0.25	1.068	0.016	1.260	0.021	0.947	0.025
	0.40	1.077	0.018	1.248	0.026	0.955	0.027

To further analyze the distribution type of structural resistance R, an examination was carried out on the outcomes of all FE simulation results to determine the distribution form of structural resistance R. Taking the load ratio of 0.20 as an example, the results are illustrated

in Figure 9. The vertical axis represents the frequency of occurrences. Consequently, a taller histogram indicates a higher frequency of occurrence. The strength coefficient ($\lambda = N_0/N_s$) represents for the axial compressive strength of CFST, which is the ratio of the FE-simulated results to the standard calculation results at standard value. It indicates that the strength coefficient λ follows a lognormal distribution for GB/T 51446-2021 [25] when the corrosion ratio standard values φ_0 are 0.15, 0.25, and 0.40, respectively. Similarly, the calculation results for Eurocode4:2004 [24] and AISC 360-16 [23] also exhibit this pattern, and the mean μ_{kp} and coefficient of variation δ_{kp} could be calculated. Consequently, it could be assumed that the distribution types of structural resistance for the three different standards follow a lognormal distribution in subsequent reliability analyses.

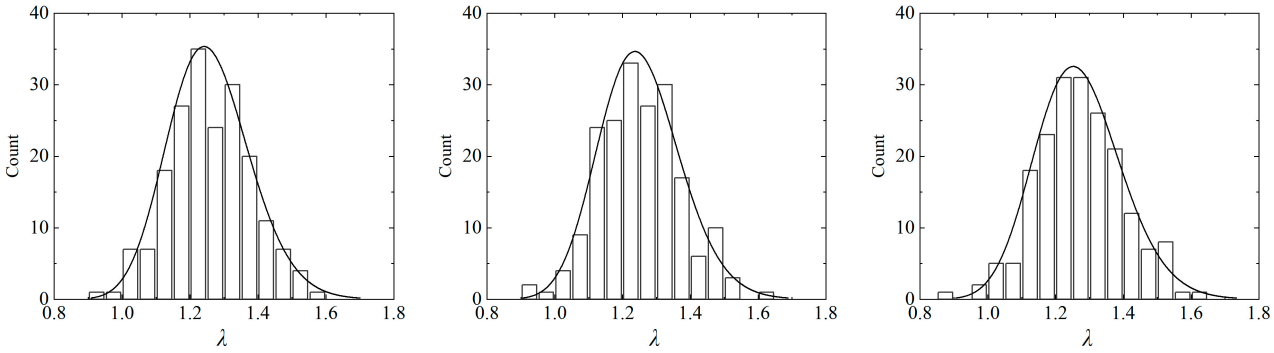

(**a**) GB/T 51446-2021 (φ_0 = 0.15) (**b**) GB/T 51446-2021 (φ_0 = 0.25) (**c**) GB/T 51446-2021 (φ_0 = 0.40)

Figure 9. Distribution of λ under different corrosion rates.

4. Reliability Analysis of Corroded CFST Members

Based on the distribution of standard calculation results, a reliability analysis could be conducted using the commonly approved methodology FOSM for corroded CFST members. This analysis can provide crucial constructional details for CFST members in wet environments.

4.1. Reliability Index Calculations with Different Standards

In accordance with Chinese standard GB/T 50283-1999 [19], structures were required to have a target reliability index β_T of 4.2 with a safety level of II and a reference period of 100 years. On the other hand, the American and European standards specify target reliability indices β_T of 3.5 and 3.8 for reference periods of 75 years and 50 years, respectively. To compare the reliability indices β obtained from different standards within the same period, the following approximate formula can be used for conversion:

$$\Phi(\beta_n) \approx [\Phi(\beta_1)]^n \tag{12}$$

where β_n is the reliability index for an n-year reference period, and β_1 is the reliability index for a 1-year reference period. The structure design typically uses a reference period of 100 years as a unified period. Therefore, the target reliability index β_T for the American standard over a reference period of 100 years is calculated as 3.4 based on Equation (12), while it is 3.65 for the European standard over the same period. The reliability index β_T for the Chinese standard is 4.2.

The calculation of reliability indices was conducted using the FOSM method, and the parameter ranges are shown in Table 9. Since steel ratio α_s has the great influence in structural performance and reliability analysis, the steel tube ratio α_s was set in a large range of 0.05 to 0.35 and divided into multiple intervals. Based on these ranges, 448 sets of parameters were computed for each of the three standards under different corrosion rates, as depicted in Figure 10. The black circles represent the calculated reliability index β, while the red solid line represents the target reliability index β_T. To ensure a fair comparison of reliability across different standards, the resistance partial factor γ was uniformly set to 1.2.

Table 9. Model parameter ranges in reliability index calculation.

Materials/Geometry/Load Parameters	Parameter Range
Load ratio η	0.20
Cube strength of the core concrete $f_{cu,c}$ (MPa)	30, 40, 50, 60, 70, 80, 90
Yield strength of the steel tube f_{ys} (MPa)	235, 355, 420, 460
Steel tube ratio α_s	0.05, 0.07, 0.09, 0.11, 0.13, 0.15, 0.17, 0.19, 0.21, 0.23, 0.25 0.27, 0.29, 0.31, 0.33, 0.35
Corrosion rate standard values φ_0	0.15, 0.25, 0.40

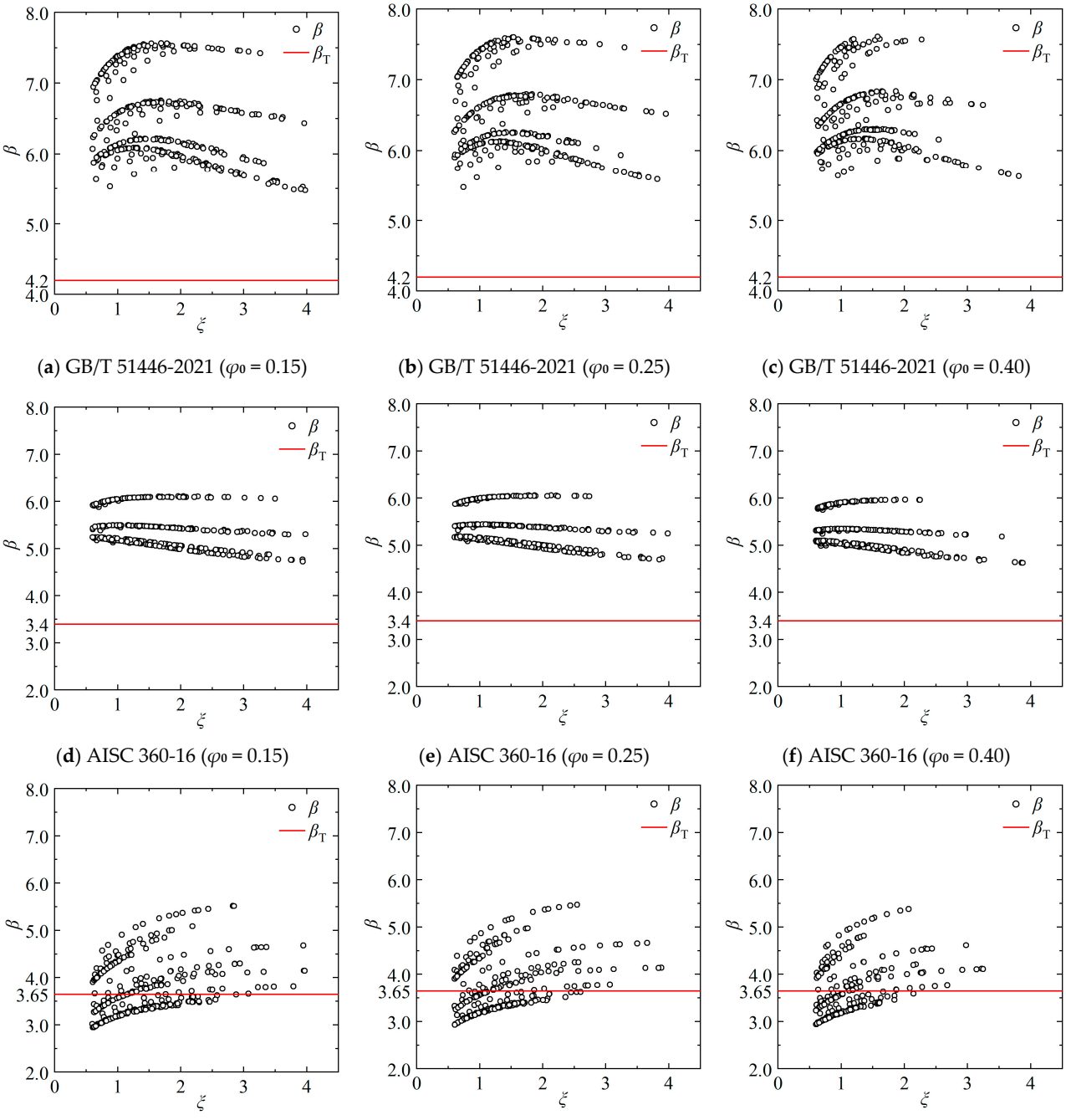

(**a**) GB/T 51446-2021 (φ_0 = 0.15) (**b**) GB/T 51446-2021 (φ_0 = 0.25) (**c**) GB/T 51446-2021 (φ_0 = 0.40)

(**d**) AISC 360-16 (φ_0 = 0.15) (**e**) AISC 360-16 (φ_0 = 0.25) (**f**) AISC 360-16 (φ_0 = 0.40)

(**g**) Eurocode4: 2004 (φ_0 = 0.15) (**h**) Eurocode4: 2004 (φ_0 = 0.25) (**i**) Eurocode4: 2004 (φ_0 = 0.40)

Figure 10. Reliability index under different standards.

Since the confinement factor ξ is an essential factor for the mechanical behaviour of CFST members, the relationship between ξ and β is illustrated in Figure 10. For Chinese standard GB/T 51446-2021 [25], the β initially increased at a high rate with the increase in ξ and decreased afterward. It could be observed that β is relatively high within the range of ξ from 1.5 to 2.0, and it gradually decreased after ξ exceeded 2.5, reaching its lowest value when ξ equalled 4.0. For AISC 360-16 [23], the pattern is obviously different. ξ had a minor influence on β, as shown in Figure 10d–f. With the increase in ξ, β remained constant initially and decreased a bit later. Finally, Eurocode4: 2004 [24] exhibits totally different results, which are shown in Figure 10g–i. Parts of the results are lower than β_T, especially when f_{ys} and $f_{cu,c}$ are high, which means the calculation method is insufficient.

In summary, the reliability index β obtained from three standards varied with changes in the confinement factor ξ. Moreover, the reliability index β from European standard Eurocode4: 2004 [24] is lower than the target reliability index β_T in some cases. Therefore, it is essential to propose structural requirements that can meet the reliability of the structure under corrosion conditions based on the results of the reliability analysis.

4.2. Reliability Analysis under Corrosion Conditions

Confinement factor ξ is composed of multiple parameters, including the strength of concrete, the strength of the steel tube, and the steel tube ratio. It is unable to independently analyze the influence pattern of a specific parameter on the reliability index β. Therefore, it is necessary to analyze the coupling effects of each parameter on β and further investigate the influence patterns. In this study, the results from Eurocode4: 2004 [24] were selected for analysis since the low reliability index β was found in the above analysis. Figure 11 illustrates the coupling influence patterns of $f_{cu,c}$, f_{ys}, and α_s on β under different corrosion rates φ_0.

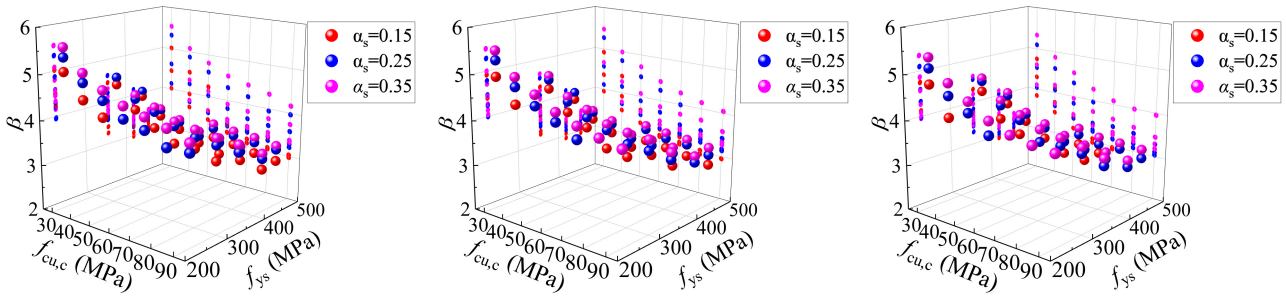

(**a**) Eurocode4: 2004 (φ_0 = 0.15) (**b**) Eurocode4: 2004 (φ_0 = 0.25) (**c**) Eurocode4: 2004 (φ_0 = 0.40)

Figure 11. Influence patterns of various parameters on β.

From Figure 11, it can be observed that the influence patterns of various parameters on β remain consistent across different corrosion rates. Therefore, this study focused on the corrosion rate of 0.15 to promote detailed analysis. As shown in Figure 11a, there is a nonlinear relationship between β and f_{ys}, and this influence pattern varies with α_s. When α_s is 0.15, β decreases by 5.53~19.96% as f_{ys} increases from 235 MPa to 420 MPa. However, β only increases by 3.03% at most as f_{ys} increases from 420 MPa to 460 MPa. When α_s is 0.35, β decreases by 19.95~24.96% as f_{ys} increases from 235 MPa to 420 MPa. The influence of f_{ys} on β becomes more noticeable as the value of α_s becomes larger. This is mainly due to the thickness of the steel tube, which increases with α_s. With a larger value of α_s, the strength contribution of the steel tube occupies a larger proportion of the entire structure. Consequently, β is more affected by the f_{ys} with the high value of α_s. The same principle applies to other parameters. For example, the influence of $f_{cu,c}$ on β is simultaneously affected by f_{ys}. When f_{ys} is 235 MPa to 420 MPa, β decreases by 12.63~23.90% as $f_{cu,c}$ increases from 30 MPa to 90 MPa. Conversely, β decreases by 4.24~6.03% with the same increase in $f_{cu,c}$ when f_{ys} is 460 MPa. As the strength of the steel tube increases sufficiently, the influence of concrete on β decreases accordingly.

Based on the comprehensive analysis, it can be concluded that f_{ys} has the greatest impact on the reliability index β. To further investigate the influence of f_{ys} and φ on β, the results with $f_{cu,c}$ of 60 MPa and α_s of 0.15 were selected for analysis, as shown in Figure 12a. To study the impact of different external loads on β under corrosion conditions, the influence of f_{ys} and φ was further analyzed under the load ratios η of 0.40 and 0.60, as shown in Figure 12b,c. This indicates that the influence of φ and f_{ys} on β is almost identical when load ratio η takes different values. Therefore, the detailed analysis will focus on the load ratio of 0.20. The following patterns can be observed:

(1) For the influence of f_{ys}, it could be found that β decreases as f_{ys} increases from 235 MPa to 420 MPa. For steel tube corrosion rates φ of 0.15, 0.25, and 0.40, β decreases by 17.79%, 18.33%, and 13.63%, respectively. Conversely, β shows a slight increase as f_{ys} increases from 420 MPa to 460 MPa. This pattern of change is highly consistent with the earlier analysis results. According to Table 2, when f_{ys} increases from 235 MPa to 420 MPa, the ratio between the mean and the standard value of f_{ys} continuously decreases. Therefore, β would decrease as f_{ys} increases from 235 MPa to 420 MPa. For f_{ys} of 420 MPa and 460 MPa, the ratio between the mean and the standard value of f_{ys} is the same, both being 0.96. Thus, β does not continue to decrease with the increase in f_{ys}.

(2) The impact of corrosion rate φ on the reliability index β is related to the yield strength of the steel tube f_{ys}. When f_{ys} is 235 MPa and 355 MPa, β decreases by 9.05% and 8.86% with the increase in φ, respectively. When f_{ys} is 420 MPa and 460 MPa, β decreases by 4.45% and 5.29% with the increasing of φ.

(3) The preceding analysis indicates that f_{ys} would lead to a reduction in reliability index β, and the minimum value of β would occur with an f_{ys} between 420 MPa and 460 MPa.

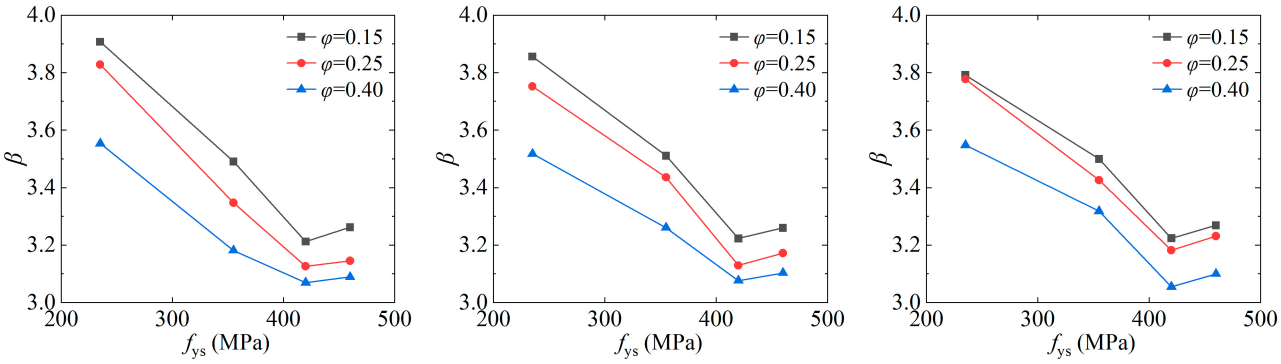

(**a**) Load ratio η = 0.20 (**b**) Load ratio η = 0.40 (**c**) Load ratio η = 0.60

Figure 12. Influence patterns of f_{ys} and φ on β.

To identify the most detrimental combination for the reliability of CFST members, it is essential to reasonably consider the coupling effects of all parameters. According to the above distribution pattern of $f_{cu,c}$ and f_{ys}, they are categorized into two groups, and the average reliability indices are calculated with an α_s of 0.15, 0.25, and 0.35. The results are presented in Table 10. The table reveals that the calculated mean reliability index β is consistently lower than the target reliability index β_T of 3.65 when f_{ys} ranges from 420 MPa to 460 MPa. Additionally, the calculated mean reliability index also falls below the target reliability index with a certain combination of α_s, f_{ys}, and $f_{cu,c}$. To ensure the reliability of CFST members under the combined effects of corrosion and external loads, it is recommended to avoid multi-parameter combinations corresponding to the bolded values of the reliability index β in Table 10. Therefore, the reliability index β under unsafe circumstances is marked in bold. In summary, the range of f_{ys} between 420 MPa and 460 MPa is generally unsafe. Additionally, particular attention should be paid when α_s is 0.15 and $f_{cu,c}$ is between 60 MPa and 90 MPa, as these conditions may also pose safety risks.

Table 10. The average reliability index under different material ranges.

α_s	f_{ys} (MPa)	$f_{cu,c}$ (MPa)	β (φ = 0.15)	β (φ = 0.25)	β (φ = 0.40)
0.15	235–355	30–60	4.23	4.24	4.15
		60–90	**3.62**	**3.55**	**3.43**
	420–460	30–60	**3.40**	**3.32**	**3.23**
		60–90	**3.11**	**3.05**	**2.99**
0.25	235–355	30–60	4.47	4.39	4.23
		60–90	3.88	3.83	3.69
	420–460	30–60	**3.58**	**3.55**	**3.45**
		60–90	**3.33**	**3.27**	**3.16**
0.35	235–355	30–60	4.56	4.56	4.44
		60–90	4.10	3.98	3.84
	420–460	30–60	**3.60**	**3.56**	**3.57**
		60–90	**3.44**	**3.39**	**3.31**

Note: The reliability index β under unsafe circumstances is marked in bold.

5. Conclusions

This study conducted a reliability study on CFST members under the coupling effects of corrosion and external compressive load. The main conclusions are as follows:

(1) Based on the experimental data of the corroded CFST, three different distribution patterns of corrosion rates were summarized. In addition, the mean values as well as the coefficients of variation under the three corrosion rates were statistically analyzed, which provides a basis for the establishment of stochastic FE models and subsequent reliability analysis.

(2) The mechanical performance of the CFST under the coupling effects of corrosion and external load was analyzed. It was found that the cube strength of core concrete $f_{cu,c}$ had the greatest impact on the maximum strength N_u. When the corrosion rate was 0.15, N_u increased by 53.30% as $f_{cu,c}$ increased from 30 MPa to 90 MPa. Further reliability analysis indicated that the yield strength of steel tube f_{ys} had the most significant impact on the reliability index β. When the corrosion rate was 0.35, β decreased by up to 24.96% as f_{ys} increased from 235 MPa to 420 MPa.

(3) Through the comprehensive analysis of CFST members under the coupling effects of the load and corrosion, it was found that the three studied standards generally ensure the reliability of the corroded CFST members in most cases. However, the calculated reliability index β could be lower than the target reliability index β_T with European standards in certain circumstances. This indicates that special attention should be given to these conditions in the design of CFST members to ensure safety and reliability.

Author Contributions: Writing—original draft preparation, D.-Y.M.; methodology and analysis, S.M.; visualization and supervision, L.-Y.X. All authors have read and agreed to the published version of the manuscript.

Funding: The authors gratefully acknowledge the financial support provided by the National Natural Science Foundation of China (52308131) and National Key R&D Program of China (2022YFC3802000).

Data Availability Statement: The original contributions presented in the study are included in the article, further inquiries can be directed to the corresponding author.

Conflicts of Interest: The authors declare no conflicts of interest.

References

1. Wu, Y.; Wang, X.; Fan, Y.; Shi, J.; Luo, C.; Wang, X. A Study on the Ultimate Span of a Concrete-Filled Steel Tube Arch Bridge. *Buildings* **2024**, *14*, 896. [CrossRef]
2. Wang, Y.; Xu, S.; Wang, H.; Li, A. Predicting the Residual Strength and Deformability of Corroded Steel Plate Based on the Corrosion Morphology. *Constr. Build. Mater.* **2017**, *152*, 777–793. [CrossRef]

3. Wang, Y.-H.; Wang, Y.-Y.; Hou, C.; Zhou, X.-H.; Deng, R.; Lan, Y.-S.; Luo, W.; Kong, W.-B. Combined Compression-Bending-Torsion Behaviour of CFST Columns Confined by CFRP for Marine Structures. *Compos. Struct.* **2020**, *242*, 112181. [CrossRef]
4. Almusallam, A.A. Effect of Degree of Corrosion on the Properties of Reinforcing Steel Bars. *Constr. Build. Mater.* **2001**, *15*, 361–368. [CrossRef]
5. Qin, S.; Cui, W. Effect of Corrosion Models on the Time-Dependent Reliability of Steel Plated Elements. *Mar. Struct.* **2003**, *16*, 15–34. [CrossRef]
6. Li, M.; Yao, L.; He, L.; Mao, X.; Li, G. Experimental Study on the Compressive Behavior of Concrete Filled Steel Tubular Columns with Regional Corrosion. *Structures* **2022**, *35*, 882–892. [CrossRef]
7. Yang, Q.; Zhao, B.; Liu, B.; Zhao, Z.; Mo, S. Influence of Corrosion on Loading Capacity of Circular Concrete-Filled Steel Tubular Column. *J. Constr. Steel Res.* **2024**, *215*, 108564. [CrossRef]
8. Zhang, F.; Xia, J.; Li, G.; Guo, Z.; Chang, H.; Wang, K. Degradation of Axial Ultimate Load-Bearing Capacity of Circular Thin-Walled Concrete-Filled Steel Tubular Stub Columns after Corrosion. *Materials* **2020**, *13*, 795. [CrossRef] [PubMed]
9. Li, W.; Han, L.-H.; Zhao, X.-L. Behavior of CFDST Stub Columns under Preload, Sustained Load and Chloride Corrosion. *J. Constr. Steel Res.* **2015**, *107*, 12–23. [CrossRef]
10. Han, L.-H.; Hou, C.; Hua, Y.-X. Concrete-Filled Steel Tubes Subjected to Axial Compression: Life-Cycle Based Performance. *J. Constr. Steel Res.* **2020**, *170*, 106063. [CrossRef]
11. Han, L.-H. *Concrete Filled Steel Tubular Structures-Theroy and Practice*, 4th ed.; Science Press: Beijing, China, 2022. (In Chinese)
12. *GB50010-2010*; Code for Design of Concrete Structures. China Architecture & Building Press: Beijing, China, 2010. (In Chinese)
13. Chen, M.-C.; Lin, B.-Y.; Huang, H. Research on the Bearing Capacity of Circular Concrete Filled Steel Tubular Short Columns. *Prog. Steel Build. Struct.* **2018**, *20*, 73–81. (In Chinese) [CrossRef]
14. Zhang, T.; Lyu, X.; Liu, H.; Zhang, L.; Wang, J.; Gao, S. Axial Performance Degradation of Squared CFST Stubs in Severe Cold and Acid Rain Area. *Constr. Build. Mater.* **2020**, *262*, 120612. [CrossRef]
15. AASHTO. *Bridge Design Specifications*; American Associaton of State Highway and Transportation Officals: Washington, DC, USA, 2012.
16. *Eurocode 0:2005*; Eurocode-Basis of Structural Design. European Committee for Standardization: Salt Lake City, UT, USA, 2002.
17. *GB 50028-2018*; Unified Standard for Reliability Design of Building Structures. China Architecture & Building Press: Beijing, China, 2018. (In Chinese)
18. Lundberg, J.E.; Galambos, T.V. Load and Resistance Factor Design of Composite Columns. *Struct. Saf.* **1996**, *18*, 169–177. [CrossRef]
19. *GB/T 50283-1999*; Unified Standard for Reliability Design of Highway Engineering Structures. China Planning Press: Beijing, China, 1999. (In Chinese)
20. Hua, Y.-X. *Performance of Concrete-Filled Steel Tubular (CFST) Members Subjected to Combined Compression (Tension)-Bending and Chloride Corrosion*; Tsinghua University: Beijing, China, 2021. (In Chinese)
21. Han, L.-H.; Hua, Y.-X.; Hou, C.; Wang, Q.-L. Circular Concrete-Filled Steel Tubes Subjected to Coupled Tension and Chloride Corrosion. *J. Struct. Eng.* **2017**, *143*, 04017134. [CrossRef]
22. *DBJ/T13-51-2010*; Technical Specification for Concrete Filled Steel Tubular Structures. The Construction Department of Fujian Province: Fuzhou, China, 2010. (In Chinese)
23. *ANSI/AISC 360-16*; Specification for Structural Steel Buildings. American Institute of Steel Construction: Chicago, IL, USA, 2016.
24. *Eurocode 4*; Design of Composite Steel and Concrete Structures-Part 1-1: General Rules and Rules for Buildings. European Committee for Standardization: Salt Lake City, UT, USA, 2004.
25. *GB/T 51446-2021*; Technical Standard for Concrete-Filled Steel Tubular Hybrid Structures. China Architecture & Building Press: Beijing, China, 2021. (In Chinese)